Journal of Electroanalytical Chemistry 932 (2023) 117240

Contents lists available at ScienceDirect

Journal of Electroanalytical Chemistry

journal homepage: www.elsevier.com/locate/jelechem

Nanoimprinted arrays of glassy carbon nanoelectrodes for improved electrochemistry of enzymatic redox-mediators

Najmeh Karimian [a,*], Davide Campagnol [a], Massimo Tormen [b], Angela Maria Stortini [a], Patrizia Canton [a], Paolo Ugo [a,*]

[a] Department of Molecular Sciences and Nanosystems, University Ca' Foscari of Venice, Via Torino 155, 30172 Venice, Italy
[b] CNR-IOM, Laboratorio TASC, Basovizza S.S. 14, Km 163.5, 34149 Trieste, Italy

ARTICLE INFO

Keywords:
Nanoelectrode
Array
Glassy carbon
Nanoimprint lithography
Redox mediator
Cyclic voltammetry

ABSTRACT

In the present study, the preparation and electrochemical application of perfectly ordered arrays of glassy carbon nanoelectrodes (GC-NEAs) is presented. After careful morphological characterization, we examined the voltammetric behaviour on GC-NEAs of some redox mediators commonly used in enzymatic electrochemical biosensors. GC-NEAs were fabricated by using nanoimprint lithography to generate ordered arrays of nanoholes, with average radius of 145 nm, onto a polycarbonate thin film deposited on a glassy carbon plate. The redox mediators examined were (ferrocenylmethyl)trimethylammonium (FA^+) as typical redox mediator for oxidase enzymes and Azure A and B as examples of mediators used for reductase enzymes. The voltammetric signals recorded indicate that the here prepared GC-NEAs operate under total overlap diffusion conditions, with an accessible potential window significantly wider than the one typical of arrays of gold nanoelectrodes. Interestingly, the electrochemical behaviour of the GC-NEAs perfectly fits with what expected on the basis of the geometrical features of the array demonstrating the role of these parameters in ruling the contribution of capacitive and faradic currents of the array which reflect in improved detection capabilities.

1. Introduction

Chemical and biochemical recognition systems are nowadays widely applied for analytical purposes, exploiting molecular recognition events to generate electrochemical signals [1–3]. Many electrochemical biosensors employ redox enzymes as recognition element for detecting the enzyme substrate as analyte or using enzymes as labels in affinity biosensors. In order to facilitate electron transfer between enzyme and the electrode surface as well as to amplify voltammetric signals by suitable electrocatalytic cycles, redox mediators are typically used [1,2]. Thanks to enhanced max fluxes, lowering of double layer charging currents and possibility of extreme miniaturization, the use of nanoelectrodes has been successfully extended to the biosensors field, showing in many cases the possibility to achieve improved bioanalytical performances [4–9].

However, the use of individual nanoelectrodes suffers for the extremely small current recorded, so that sophisticated electronic amplification of signals and accurate shielding from external electric fields is required. This limit can be overcome by using arrays of nanoelectrodes. Random distributed arrays, also named nanoelectrode ensembles (NEEs), were originally prepared by electroless [4,9–12] or electrochemical deposition of gold or other metals [13–16]. Notwithstanding the biocompability and chemical inertness of gold as electrode material, the use of nanogold suffers from some limits related to the relatively narrow potential window accessible which, on the cathodic side is limited by facilitated hydrogen evolution and, on the anodic side, by facilitated gold oxides formation [4,17]. For the case of NEEs, the spatial distribution of the nanoelectrodes is random arranged, consequently the diffusion regime is not always fully controllable, possibly changing from total overlap to pure radial or to mixed [4,18–20] by changing the scan rate or the viscosity of the matrix in the electrochemical cell [21,22]. These limits prompted to the development of ordered nanoelectrode arrays (NEAs). NEAs have been prepared by top-down lithographic methods such as ion beam lithography [23], electron beam lithography (EBL) [24–26] and scanning probe lithography [27]. Among these nanofabrication techniques, electron beam lithography (EBL) showed to be suitable to produce ordered nanostructures with sub-50 nm spatial resolution and well-defined topographical features [26]. NEAs were initially prepared using gold substrates but later, to widen the accessible potential win-

* Corresponding authors.
E-mail addresses: najmeh.karimian@unive.it (N. Karimian), ugo@unive.it (P. Ugo).

https://doi.org/10.1016/j.jelechem.2023.117240
Received 23 December 2022; Received in revised form 26 January 2023; Accepted 31 January 2023
Available online 3 February 2023

dow and to improve chemical robustness, boron doped diamond (BDD) was used [28]. Unfortunately, the EBL process used to fabricate these arrays is expensive and time consuming, therefore unsuitable for large-scale production of electrochemical sensors. This limit can be overcome by using nanoimprinting lithography (NIL) [24,29,30], which relies on direct mechanical deformation of a suitable polymeric material allowing to achieve resolutions in the nanometer range [30]. In the NIL process, a specific nanostructured mold is used to indent the same nanostructures in a thin thermoplastic film deposited on a substrate while the latter is in a melt state, i.e., during a thermomechanical cycle. This method can be used to generate arrays of nanoholes which can act as slightly recessed nanoelectrodes [31], as schematized in Supplementary Material, Scheme S1. Polycarbonate was used by Tormen and co-workers as the polymeric layer on which the nanoholes were imprinted on BDD substrates. The obtained arrays combined the improved electroanalytical properties of BDD nanoelectrodes [32,33] with the possibility to use the polycarbonate layer between the nanoelectrodes as anchoring substrate for the immobilization of biomacromolecules [6–8,34,35]. Considering the high cost and complex preparation of BDD substrates as well as the possible local variation at the nanoscale of the properties of this material because of its nanocrystalline structure [36,37], a valid and less expensive alternative is offered by glassy carbon (GC). GC is widely used as electrode material thanks to its high chemical and mechanical stability, negligible porosity, excellent conductivity and, more importantly, wide accessible potential window [38,39]. This notwithstanding, the use of carbon materials (even different from GC) for the preparation of ordered arrays of nanosized electrodes is quite limited [40–44]. In particular, Lentz et al. [45] described the template preparation of glassy carbon nanowires. It was demonstrated that it is the overall delocalized charge carrier density which determines the conductivity of the system, this parameter depending strongly on the morphology and thermal treatment of the nanowires which exhibited not ideal electron conduction properties at the nanoscale.

Therefore, for electrochemical sensing application other nanofabrication strategies should be considered, suitable to preserve the excellent electrochemical properties of bulk GC. On this research line, C. Wang et al. [46], proposed the fabrication of arrays of GC nanoelectrodes with 20–120 nm radius by exploiting the self-assembly of amphiphilic block copolymer onto a GC bulk substrate. Local dissolution of the most soluble component of the co-polymer generated nanoholes which act as nanoelectrodes.

In the present research, we improved the nanofabrication of arrays of GC nanoelectrodes by applying thermal nanoimprinting lithography, which allows high production yield combined with high spatial resolution in nanofabrication. By nanoimprinting arrays of nanoholes in a thin layer of polycarbonate deposited in GC platelets, it was possible to prepare arrays of shallow recessed GC nanoelectrodes arranged in ordered square lattice with a relatively small pitch/radius ratio, around 5. With such a geometry, a large number of electrodes is contained within a relatively small geometric area, so providing high Faradaic currents with small capacitive contribution and minimizing at the same time, edge effects which depend on the percentage of nanoelectrodes at the periphery of the array. At the best of our knowledge, this is the first report presenting the preparation and electroanalytical use of perfectly ordered arrays of GC nanoelectrodes (GC-NEAs).

The electrochemical performances of the GC-NEAs were studied using some redox mediators, commonly used in enzymatic electrochemical biosensors, testing ferrocenyl methyl trimethylammonium (FA^+) as example of mediator for oxidase enzymes [47,48] while two phenothiazines, namely Azure A and B, were studied as examples of redox mediators for reductase enzymes [17,48]. Since FA^+ undergoes fast electron transfer, providing highly reversible voltammetric patterns characterized by known electrochemical parameters, its use allowed us to perform the careful electrochemical characterization of the GC-NEA, obtaining data which well matched the expectations based on the geometrical features of the array. For phenothiazine mediators, the goal was to evaluate possible advantages coming from the use of GC-NEAs vs arrays of noble metal nanoelectrodes, thanks to the wider potential window hopefully accessible with GC nanoelectrodes.

2. Materials and methods

2.1. Chemicals and materials

Polycarbonate solution (4 % w/v) was obtained by dissolution of solid polycarbonate Makrolon (Bayer Sheet Europe, Darmstadt, Germany) in cyclopentanone. Glassy carbon platelets by Tokai Carbon, Tokyo, Japan, thickness 3 mm, cut to approximately a size of 10 × 20 mm (width × length) were used as GC substrate for the NEA fabrication.

The phenothiazines Azure A and Azure B were purchased from Sigma-Aldrich. Standard stock solutions of Azure A and Azure B (2 mM) were prepared in phosphate buffer saline solution (PBS 1X: 1×10^{-2} M phosphate buffer, 1.37×10^{-1} M NaCl, 2.7×10^{-3} M KCl, pH 7.4 @ 25 °C). Ferrocenylmethyl trimethylammonium hexafluorophosphate (FA^+PF6^-) was prepared as follows: ferrocenylmethylamine (Aldrich) was first reacted with methyl iodide to form the quaternary ammonium iodide [49] to be later converted to FA^+PF6^- by reaction with $AgPF_6$. A 0.1 mM FA^+ solution was prepared in PBS 1X. All other reagents were of analytical grade and solutions were prepared using Milli_Q water.

2.2. Instrumentation and methods

Cyclic voltammetry (CV) measurements were performed at room temperature with CH Instruments potentiostats (CH660B and CH1222a), controlled via personal computer by CHI software. Measurements were performed in a three-electrode cell, using the GC-NEA as the working electrode, a Pt spiral counter electrode and an aqueous Ag|AgCl|KCl (sat.) reference electrode to which all here reported potential values are referred. The sample solution was purged with purified nitrogen for 15 min and was held under a nitrogen atmosphere during the measurements. Scanning Electron Microscopy (SEM) measurements were done using a Sigma-VP FE-SEM (Zeiss) equipped with a high-resolution in-lens Secondary Electrons (SE) detector and an Everhart-Thornley SE detector.

2.3. Fabrication of nanoelectrodes arrays

GC-NEAs were kindly provided by ThunderNIL S.r.L., Basovizza, Trieste (Italy). For the nanoimprint lithography process, a stamp was used composed by an array of nanopillars obtained by replicating a commercial silicon master consisting of a square array of nanoholes. The polycarbonate film was patterned by indenting the pillars in the PC, i.e., forcing the displacement of the polymer from the area of the pillars on the stamp during the NIL thermomechanical cycle. Details on the fabrication of the stamp are carefully described elsewhere [31] and summarized in Scheme S1 in Supplementary Material.

Arrays of nanoelectrodes were fabricated by NIL, applying to GC platelets the procedure described previously for BDD thin film electrodes [31]. Briefly, a polycarbonate film was spin-coated at 2000 rpm on a thick layer of GC prepared by pyrolysis of a polymeric photoresist. The polycarbonate film was annealed for 30 min at 180 °C to remove residual solvent. The average film thickness of PC films prepared from solutions at 4 % in cyclopentanone, measured by profilometry, was 200 nm. To ensure the indentation of the nanoarray structures, a pressure of 10 MPa was applied to the stack of stamp/polycarbonate film/macroelectrode on a 25 × 25 mm^2 for 10 min at 180 °C (release temperature of 80 °C). Eventual residuals of PC present

in the holes were removed by treating the nanoarray with oxygen plasma for 4 s using an ICP-RIE system applying 4 mTorr pressure, 200 W coil power and 10 W platen power. After this treatment the thickness of the PC layer lowers to 180 nm and the final recess degree (L) of the nanoelectrodes is: L = (recess length/nanoelectrode radius) = 1.2.

Finally, in order to expose to the electrolyte solution a surface with known geometric area, the plate with the GC-NEA was coated with insulating tape apart a hole of 3 mm diameter, punched in the tape. The macro-structure of the GC-NEA is shown in Scheme S2 in Supplementary Materials.

3. Results and discussion

3.1. Morphological characterization of NEAs

The morphology and geometrical features of fabricated GC-NEAs were carefully characterized by FE-SEM analysis. Data shown in Fig. 1 were obtained at 10 kV collecting secondary electron with Everhart-Thornley (A) and in-lens (B) detectors. Both images confirm the preparation of perfectly ordered arrays of glassy carbon electrodes, that are the black nanoholes imprinted onto the polycarbonate layer in the SEM images. Analysis of the data indicate that the nanoelectrodes have a radius of 145 ± 5 nm (average ± standard deviation) and are arranged in a square lattice with 770 nm pitch.

These data allowed us to calculate the fractional area, *f*, given as:

$$f = A_{act}/A_{geom} \quad (1)$$

where A_{act} is the exposed GC surface of the nanoelectrodes and A_{geom} is the overall geometric area composed by the GC nanoelectrodes and the PC surrounding them. By simple geometrical considerations, the *f* value calculated from the above FE-SEM data is $f = 0.11$. As detailed below, the *f* value is important for evaluating the ratio between the capacitive current (main component of the voltammetric noise) and the faradaic current (useful analytical signal) to which the detection capabilities of voltammetry are related [4,7,17].

3.2. Electrochemical characterization

3.2.1. Evaluation of the voltammetric behaviour of FA^+ at the NEA

The A_{act} of the GC-NEAs can be measured experimentally by performing cyclic voltammetry measurements (CV) in pure supporting electrolyte alone (10 mM PBS 1X, pH 7.4). Under these conditions the current recorded is the double layer capacitive current [4,50,51] which depends on the scan rate and A_{act} according to equation:

$$I_c = C_{dl} \times A_{act} \times v \quad (2)$$

where I_c is the capacitive current, C_{dl} is the double layer capacitance and v is the scan rate.

By recording a series of blank voltammograms at different scan rates, the *Ic* vs v plot provides a straight line whose slope is equal to $C_{dl} \times A_{act}$.

Fig. 2A shows the voltammograms recorded with the GC-NEA in 10 mM PBS 1X, pH 7.4, changing the scan rate from 0.005 to 0.100 V s^{-1}. Fig. 2B presents the dependence of the capacitive current (I_c) measured as the half-difference between the anodic and cathodic current at + 0.45 V, as a function of the scan rate (v) [4,52,53].

In the literature, C_{dl} value for glassy carbon ranges approximately between 35 and 55 μF cm^{-2} [54,55]. Assuming an average value of 45 μF cm^{-2}, substitution into Eq. (2) allowed us to calculate an experimental A_{act} value of 0.012 cm^2.

In order to take the maximum advantage of the improved electrochemical performances of NEAs with respect to conventional electrodes, the use of redox probes with very fast electron transfer kinetics is recommended [4,56]. Note that FA^+, as well as other ferrocenyl derivatives, are widely used as redox mediators for enzymatic biosensors, in particular for shuttling electrons in sensors which employ oxidase enzymes, such as glucose oxidase [8,51]. Fig. 3A reports the peaks shaped cyclic voltammograms recorded with a GC-NEA in a solution containing 100 μM FA^+ in 10 mM PBS 1X, pH 7.4 at different scan rates. Relevant voltammetric parameters measured from these CVs are listed in Table S1. The plot for the anodic and cathodic peak currents (*Ip*) vs the square root of the scan rate ($v^{1/2}$) reported in Fig. 3B shows a linear trend, typical for an electrochemical process controlled by semi-infinite linear diffusion.

All these evidences indicate that the GC-NEAs operate under total overlap diffusion conditions [4,7], in agreement with the relatively small pitch/radius ratio for the nanoelectrodes in the NEA used here. Note that in total overlap regime the effect of the slight recession of the nanoelectrods in the array does not influence the overall Faradaic current recorded by the array [20,57]. The here observed electrochemical oxidation of FA^+ at the GC-NEA presents the feature typical for a one-electron reversible (Nernstian) electrochemical process in which the rate of reaction is ruled by the diffusion of the electroactive species to the surface of the overall array.

It was demonstrated that at arrays of nanoelectrodes operating under total overlap diffusion conditions, the peak current obeys the Randles-Sevcik equation (Eq. (3)), adapted by taking in account the geometric area of the NEA [4,17]:

$$Ip = 2.69 \times 10^5 n^{3/2} A_{geom} D^{1/2} C^* v^{1/2} \quad (3)$$

where n is the number of transferred electron ($n = 1$ for FA^+), C^* is the bulk concentration of the electroactive species (FA^+) in moles/cm^3, D is the FA^+ diffusion coefficient, that is 4 × 10^{-6} cm^2 s^{-1} [4].

The geometric area of the GC-NEA, calculated from the slope of the *Ip* vs $v^{1/2}$ plot (see Fig. 3A and Fig. 3B, resulted equal to 7.0 × 10^{-2} cm^2. The experimental fractional area calculated as the ratio between

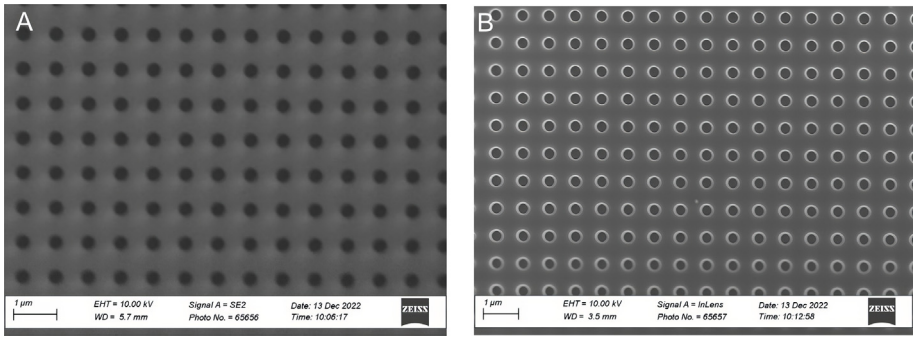

Fig. 1. FE-SEM Images of the GC-NEA surface, magnification 20,000×, 10 kV, obtained collecting secondary electron with Everhart-Thornley (A) and in-lens (B) detectors.

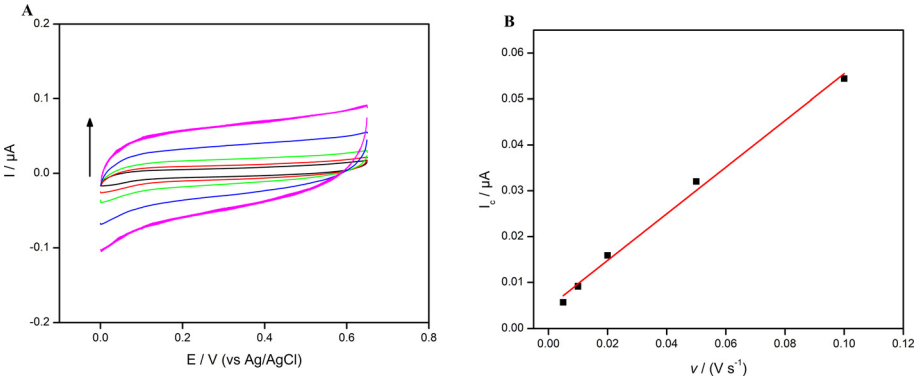

Fig. 2. (A) Background cyclic voltammograms recorded in PBS 1X (10 mM, pH 7.4) at a GC-NEA at different scan rates, from the outer to the inner: 0.100 V s^{-1}, 0.050 V s^{-1}, 0.020 V s^{-1}, 0.010 V s^{-1}, 0.005 V s^{-1}; (B) Linear correlation between capacitive currents and scan rate.

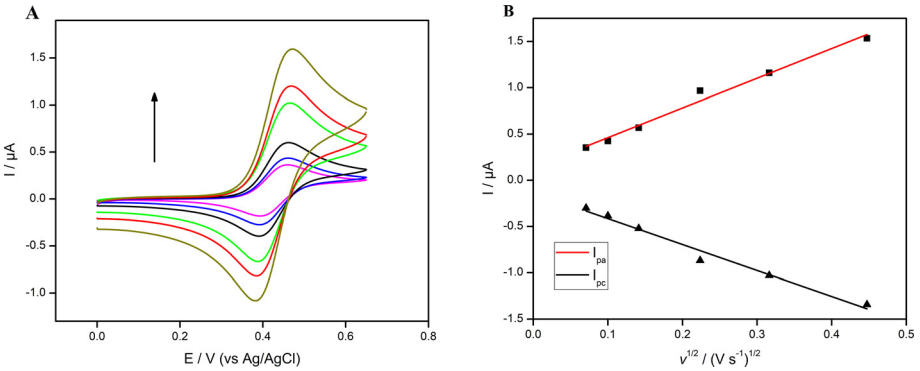

Fig. 3. (A) Voltammograms recorded at a solution of 100 μM FA^+ in 10 mM PBS 1X, pH 7.4 at a GC-NEA at different scan rates; from the outer to the inner 0.200 V s^{-1}, 0.100 V s^{-1}, 0.050 V s^{-1}, 0.020 V s^{-1}, 0.010 V s^{-1}, 0.005 V s^{-1}(B) Linear correlation between faradic peak currents and square root of scan rate.

the experimentally determined values for the active and geometric area, results:

$$f = A_{act}/A_{geom} = 0.012/0.070 = 0.17$$

Interestingly, this f value obtained from electrochemical data is in satisfactory agreement with the f value evaluated by geometrical calculations.

These results confirm: i) the reliability of the electrochemical characterization of the GC-NEA; ii) the perfect control of features of the GC-NEA fabricated by NIL; iii) the reversibility of the electrochemical behaviour of the FA^+ redox mediator on this kind of arrays.

3.2.2. Cathodic electrochemistry of NEA with phenothiazine redox mediators

The fabricated GC-NEAs were tested cathodically using two electron-transfer mediators used for reductase enzymes, namely the two phenothiazines Azure A and Azure B. The electrochemical behaviour of these mediators is more complex and less "ideal" than the one of FA^+ for the following reasons [17]:

(i) the electrochemical reduction of the mediators occurs at negative potential values, so that it can overlap with the reduction of the hydronium ion (H_3O^+), in particular on electrode materials with low hydrogen evolution overpotential, such as Au or Pt;
(ii) Azure A and Azure B can adsorb on electrode surfaces;
(iii) the electrochemical reduction of these mediators is influenced by the pH of the solution, according to Scheme 1:

Fig. 4A reports the cyclic voltammograms recorded at different scan rates with the GC-NEA in PBS solution containing 75 μM Azure B. The CV are characterized by a cathodic peak at approximately −0.250 mV vs Ag/AgCl with associated anodic peak at −0.220 mV vs Ag/AgCl; these and other CV parameters measured from these voltammograms are listed in Table S2.

Interestingly, at a potential value as negative as −0.6 V vs Ag/AgCl, no proton reduction occurs at the GC-NEA. Note that, in a similar study performed previously using ensembles of gold nanoelectrodes (NEEs) [17], in PBS, pH 7.4, the water proton reduction started to occur already at −0.2 V vs Ag/AgCl.

As a consequence, the CV signal for Azure B recorded with the GC-NEA is significantly better resolved from the background current than the signals presented in the literature with Au-NEE (see ref. [17]), confirming the efficiency of the GC-NEA in eliminating the interference of the hydrogen evolution reaction and the widening of the cathodic limit of the accessible potential window.

Fig. 4B shows the log I_{pc} vs log v plot which results linear, with a slope equal to 0.55. All these data agree with the occurrence of a two-electron process controlled by semi-infinite planar diffusion, indicating again the operativity of the total overlap diffusion control for the reduction of Azure B at array of GC nanoelectrodes.

Fig. 5A reports the cyclic voltammograms recorded at 20 mV s^{-1} with the GC-NEA at increasing concentrations of Azure B, from 5 nM to 42 μM. The current of the cathodic peak increases, in absolute value, linearly with the Azure B concentration (Fig. 5B), with a sensitivity (slope) of −0.027 μA μM^{-1}. Note that the Azure B signal is distinguishable from the background current already at tens nM concentration values, indicating improved detection capabilities for the GC-NEA.

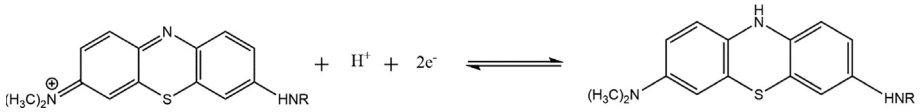

Scheme 1. Electrochemical reduction of phenothiazine mediators where: R = H for Azure A; R = CH_3 for Azure B [17].

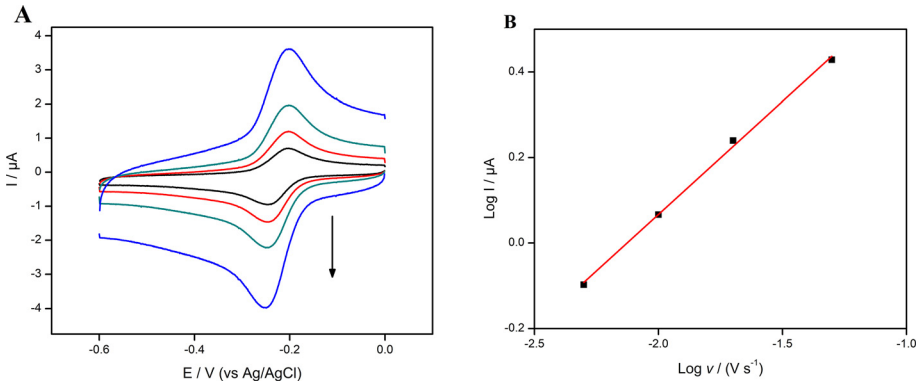

Fig. 4. (A) Cyclic voltammograms recorded with GC-NEA in the presence of 75 µM Azure B in 10 mM PBS 1X, pH 7.4 at different scan rates from inner to outer 0.005, 0.010, 0.020, 0.050 V s^{-1}. (B) Linear correlation between logarithm of the cathodic current and logarithm of the scan rate.

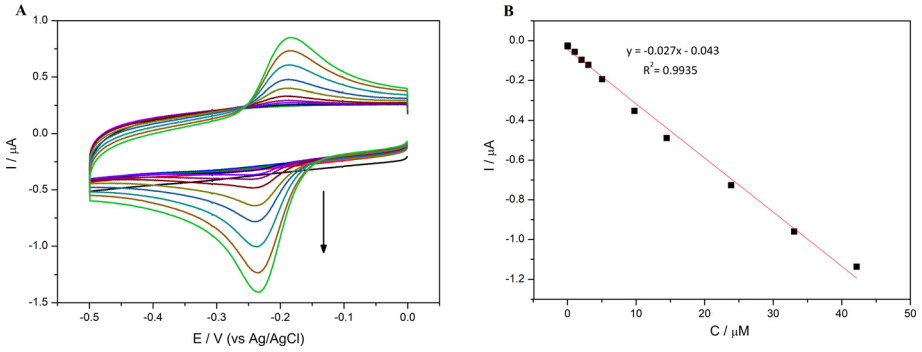

Fig. 5. (A) Cyclic voltammograms recorded at a GC-NEA in the presence of 0, 0.005, 0.01, 0.02, 0.05, 1.05, 2.05, 3.05, 5.05, 9.8, 14.5, 23.9, 33.1, 42.0 µM Azure B; scan rate = 0.020 V s^{-1}; supporting electrolyte: 10 mM PBS 1X, pH 7.4. (B) Dependence of the cathodic peak current on Azure B concentration (calibration plot).

Fig. S1 in Supplementary Material reports the CV patterns recorded with the GC-NEA at different scan rates in 75 µM Azure A solution at pH 7.4. These voltammograms are substantially comparable with those obtained for Azure B, even if the peak-to-peak separation is a bit larger, suggesting a slightly lower degree of electrochemical reversibility for Azure A. Anyhow, the CVs obtained confirm the satisfactory behaviour of the GC-NEA in promoting the cathodic electrochemistry of this class of redox mediators.

4. Conclusions

GC-NEAs prepared by nanoimprinting lithography present interesting features, in particularly for their use as sensing platforms for enzymatic (as well as for other kind of) electrochemical biosensors. The fabrication procedure provides indeed perfectly ordered arrays of nanodot electrodes with electrochemical behaviour which fits with their geometrical features. The use of nanoimprint lithography allows the quick preparation of NEAs containing a huge number of nanoelectrodes, thus making negligible the edge effects that, instead, play a relevant role in controlling the electrochemical response for the case of NEAs composed by very small numbers of nanoelectrodes [25,58]. The value of the fractional electrode area *f* for the here presented GC-NEAs is in the 0.1 range, that means that the faradaic/capacitive current ratio is improved at least one order of magnitude with respect to a regular electrode with the same geometric area of the GC-NEA [4,7]. Of course, by changing the geometry of array e.g. by increasing the distance between the nanoelectrodes, it can be possible to prepare arrays operating under pure radial control conditions. Such a change of geometry could further improve the signal/noise ratio, but at the expense of the possibility to prepare miniaturized arrays able to provide high (i.e. easily detectable) Faradaic currents even for small analyte concentrations (micromolar or lower). For the GC-NEAs here studied, the Faradaic/capacitive current ratio is independent on the A_{geom} value, so that, in principle, they can be easily miniaturized, down to hundreds micrometre radius of the overall array, or even enlarged, without any loss in analytical performances [47]. Interestingly for electroanalytical applications, the use of GC as the electroactive material for arrays of nanoelectrodes, allows the significant widening of the accessible potential window, in particular in cathodic direction. Note that an important feature supporting the usefulness of GC-NEA towards the development of advanced integrated biosensors, is that in NEA the biorecognition element can be easily immobilized on the polycarbonate of the array, keeping the nanoelectrodes clean to best perform the function of electrochemical transducers [6,31,34,35].

A final note concerns the fact that in enzymatic biosensors the mediator is typically added in excess with respect to the enzyme [1],

so that the capability of GC-NEAs to detect sub-micromolar concentrations of mediator, in principle, should allow one to build electrochemical biosensors which employ extremely small concentration of the enzymatic component.

CRediT authorship contribution statement

Najmeh Karimian: Methodology, Validation, Data curation, Writing – review & editing, Supervision, Project administration. **Davide Campagnol:** Methodology, Validation, Data curation, Writing – review & editing. **Massimo Tormen:** Conceptualization, Methodology, Validation, Resources, Data curation, Writing – review & editing. **Angela Maria Stortini:** Methodology, Resources, Project administration. **Patrizia Canton:** Resources, Validation, Data curation. **Paolo Ugo:** Conceptualization, Methodology, Resources, Data curation, Writing – review & editing, Supervision, Project administration.

Data availability

Data will be made available on request.

Declaration of Competing Interest

The authors declare that they have no known competing financial interests or personal relationships that could have appeared to influence the work reported in this paper.

Acknowledgments

D.C. was the grateful recipient of a PhD studentship by Biofield Innovation S.R.L. (Padua, Italy).

Appendix A. Supplementary data

Supplementary data to this article can be found online at https://doi.org/10.1016/j.jelechem.2023.117240.

References

[1] P. Ugo, P. Marafini, M. Meneghello, Bioanalytical chemistry-from biomolecular recognition to nanobiosensing, De Gruyter, Berlin, 2021. doi: 10.1515/9783110589160.
[2] N.J. Ronkainen, H.B. Halsall, W.R. Heineman, Electrochemical biosensors, Chem. Soc. Rev. 39 (2010) 1747–1763, https://doi.org/10.1039/B714449K.
[3] A. Singh, A. Sharma, A. Ahmed, A.K. Sundramoorthy, H. Furukawa, S. Arya, A. Khosla, Recent advances in electrochemical biosensors: applications, challenges, and future scope, Biosensors 11 (2011) 336–366, https://doi.org/10.3390/bios11090336.
[4] V.P. Menon, C.R. Martin, Fabrication and evaluation of nanoelectrode ensembles, Anal. Chem. 67 (1995) 1920–1928, https://doi.org/10.1021/ac00109a003.
[5] D.W.M. Arrigan, Nanoelectrodes, Nanoelectrode arrays and their applications, Analyst 129 (2004) 1157–1165, https://doi.org/10.1039/B415395M.
[6] S. Pozzi Mucelli, M. Zamuner, M. Tormen, G. Stanta, P. Ugo, Nanoelectrode ensembles as recognition platform for electrochemical immunosensors, Biosens. Bioelectron. 23 (2008) 1900–1903, https://doi.org/10.1016/j.bios.2008.02.027.
[7] M. Ongaro, P. Ugo, Bioelectroanalysis with nanoelectrode ensembles and arrays, Anal. Bioanal. Chem. 405 (2013) 3715–3729, https://doi.org/10.1007/s00216-012-6552-z.
[8] N. Karimian, P. Ugo, Recent advances in sensing and biosensing with arrays of nanoelectrodes, Curr. Opin. Electrochem. 16 (2019) 106–116, https://doi.org/10.1016/j.coelec.2019.04.026.
[9] R. Gasparac, B.J. Taft, M.A. Lapierre-Devlin, A.D. Lazareck, J.M. Xu, S.O. Kelley, Ultrasensitive electrocatalytic DNA detection at two- and three-dimensional nanoelectrodes, J. Am. Chem. Soc. 126 (2004) 12270–12271, https://doi.org/10.1021/ja0458221.
[10] M. Delvaux, S. Demoustier-Champagne, A. Walcarius, Flow injection amperometric detection at enzyme-modified gold nanoelectrodes, Electroanalysis 16 (2004) 190–198, https://doi.org/10.1002/elan.200402778.
[11] K. Krishnamoorthy, C.G. Zoski, Fabrication of 3D gold nanoelectrode ensembles by chemical etching, Anal. Chem. 77 (2005) 5068–5071, https://doi.org/10.1021/ac050604r.
[12] R.J. Gilliam, S.J. Thorpe, D.W. Kirk, A nucleation and growth study of gold nanowires and nanotubes in polymeric membranes, J. Appl. Electrochem. 37 (2006) 233–239, https://doi.org/10.1007/s10800-006-9240-x.
[13] C. Schonenberger, B.M.I. van der Zande, L.G.J. Fokkink, M. Henny, C. Schmid, M. Kruger, A. Bachtold, R. Huber, H. Birk, U. Staufer, Template synthesis of nanowires in porous polycarbonate membranes: electrochemistry and morphology, J. Phys. Chem. B 101 (1997) 5497–5505, https://doi.org/10.1021/jp963938g.
[14] P. Forrer, F. Schlottig, H. Siegenthaler, M. Textor, Electrochemical preparation and surface properties of gold nanowire arrays formed by the template technique, J. Appl. Electrochem. 30 (2000) 533–541, https://doi.org/10.1023/A:1003941129560.
[15] M.G. Insinga, R.L. Oliveri, C. Sunseri, R. Inguanta, Template electrodeposition and characterization of nanostructured Pb as a negative electrode for lead-acid battery, J. Power Sources 413 (2019) 107–116, https://doi.org/10.1016/j.jpowsour.2018.12.033.
[16] A. Gambirasi, S. Cattarin, M. Musiani, L. Vázquez-Gómez, E. Verlato, Direct electrodeposition of metal nanowires on electrode surface, Electrochim. Acta 56 (2011) 8582–8588, https://doi.org/10.1016/j.electacta.2011.07.045.
[17] B. Brunetti, P. Ugo, L.M. Moretto, C.R. Martin, Electrochemistry of phenothiazine and methylviologen biosensor electron-transfer mediators at nanoelectrode ensembles, J. Electroanal. Chem. 491 (2000) 166–174, https://doi.org/10.1016/S0022-0728(00)00169-8.
[18] C. Amatore, J.M. Saveant, D. Tessier, Charge transfer at partially blocked surfaces- a model for the case of microscopic active and inactive sites, J. Electroanal. Chem. 147 (1983) 39–51, https://doi.org/10.1016/S0022-0728(83)80055-2.
[19] J.C. Hulteen, V.P. Menon, C.R. Martin, Template preparation of nanoelectrode ensembles achieving the 'pure-radial' electrochemical response limiting case, J. Chem. Soc. Faraday Trans. 92 (1996) 4029–4032, https://doi.org/10.1039/Ft9969204029.
[20] J. Guo, E. Lindner, Cyclic Voltammograms at coplanar and shallow recessed microdisk electrode arrays: guidelines for design and experiment, Anal. Chem.. 81 (2009) 130–138, https://doi.org/10.1021/ac801592j.
[21] M. De Leo, L.M. Moretto, O. Buriez, P. Ugo, Electrochemical behavior of nanoelectrode ensembles in the ionic liquid [BMIm][BF4], Electroanalysis 21 (2009) 392–398, https://doi.org/10.1002/elan.200804414.
[22] P. Ugo, L.M. Moretto, M. De Leo, A. Doherty, C. Vallese, S. Pentlavalli, Diffusion regimes at nanoelectrode ensembles in different ionic liquids, Electrochim. Acta 55 (2010) 2865–2872, https://doi.org/10.1016/j.electacta.2009.12.059.
[23] Y.H. Lanyon, G. De Marzi, Y.E. Watson, A.J. Quinn, J.P. Gleeson, G. Redmond, D. W.M. Arrigan, Fabrication of nanopore array electrodes by focused ion beam milling, Anal. Chem. 79 (2007) 3048–3055, https://doi.org/10.1021/ac061878x.
[24] M.E. Sandison, J.M. Cooper, Nanofabrication of electrode arrays by electron-beam and nanoimprint lithographies, Lab Chip 6 (2006) 1020–1025, https://doi.org/10.1039/b516598a.
[25] L.M. Moretto, M. Tormen, M. De Leo, A. Carpentiero, P. Ugo, Polycarbonate-based ordered arrays of electrochemical nanoelectrodes obtained by e-beam lithography, Nanotechnology 22 (18) (2011) 185305.
[26] F. Virgilio, M. Prasciolu, P. Ugo, M. Tormen, Development of electrochemical biosensors by e-beam lithography for medical diagnostics, Microelectron. Eng. 111 (2013) 320–324, https://doi.org/10.1016/j.mee.2013.02.026.
[27] E. Albisetti, D. Petti, M. Pancaldi, M. Madami, S. Tacchi, J. Curtis, W.P. King, A. Papp, G. Csaba, W. Porod, P. Vavassori, E. Riedo, R. Bertaccoet, Nanopatterning reconfigurable magnetic landscapes via thermally assisted scanning probe lithography, Nat. Nanotechnol. 11 (2016) 545–551, https://doi.org/10.1038/nnano.2016.25.
[28] M. Sentic, F. Virgilio, A. Zanut, D. Manojlovic, S. Arbault, M. Tormen, N. Sojic, P. Ugo, Microscopic imaging and tuning of electrogenerated chemiluminescence with boron-doped diamond nanoelectrode arrays, Anal. Bioanal. Chem. 408 (2016) 7085–7094, https://doi.org/10.1007/s00216-016-9504-1.
[29] S.Y. Chou, P.R. Krauss, P.J. Renstrom, Imprint of sub-25 nm vias and trenches in polymers, Appl. Phys. Lett. 67 (21) (1995) 3114–3116.
[30] L.J. Guo, Nanoimprint lithography: methods and material requirements, Adv. Mater. 19 (2007) 495–513, https://doi.org/10.1002/adma.200600882.
[31] A. Zanut, A. Cian, N. Cefarin, A. Pozzato, M. Tormen, Nanoelectrode arrays fabricated by thermal nanoimprint lithography for biosensing application, Biosensors 10 (2020) 90–101, https://doi.org/10.3390/bios10080090.
[32] M. Hupert, A. Muck, J. Wang, J. Stotter, Z. Cvackova, S. Haymond, Y. Show, G.M. Swain, Conductive diamond thin-films in electrochemistry, Diam. Relat. Mater. 12 (2003) 1940–1949, https://doi.org/10.1016/S0925-9635(03)00260-7.
[33] C. Dincer, R. Ktaich, E. Laubender, J.J. Hees, J. Kieninger, C.E. Nebel, J. Heinze, G. A. Urban, Nanocrystalline boron-doped diamond nanoelectrode arrays for ultrasensitive dopamine detection, Electrochim. Acta 185 (2015) 101–106, https://doi.org/10.1016/j.electacta.2015.10.113.
[34] F. Bottari, P. Oliveri, P. Ugo, Elelctrochemcial immunosensor based on nanoelectrode ensembles for immunoglobulin IgY detection: application to identify hen's egg yolk in temepra paintings, Biosens. Bioelectron. 52 (2014) 403–410, https://doi.org/10.1016/j.bios.2013.09.025.
[35] M. Silvestrini, L. Fruk, P. Ugo, Functionalized ensembles of nanoelectrodes as affinity biosensors for DNA hybridization detection, Biosens. Bioelectron. 40 (2013) 265–270, https://doi.org/10.1016/j.bios.2012.07.041.
[36] S. Gupta, O.A. Williams, E. Bohannan, Electrostatic force microscopy studies of boron-doped diamond films, J. Mater. Res. 22 (2007) 3014–3028, https://doi.org/10.1557/JMR.2007.0229.
[37] V.D. Blank, M.S. Kuznetsov, S.A. Nosukhin, S.A. Terentiev, V.N. Denisov, The influence of crystallization temperature and boron concentration in growth

environment on its distribution in growth sectors of type IIb diamond, Diamond Rel. Mater. 16 (2007) 800–804, https://doi.org/10.1016/j.diamond.2006.12.010.
[38] R.L. McCreery, Advanced carbon electrode materials for molecular electrochemistry, Chem. Rev. 108 (2008) 2646–2687, https://doi.org/10.1021/cr068076m.
[39] V. Uskokovic, A historical review of glassy carbon: synthesis, structure, properties, and applications, Carbon Trends 5 (2021) 100116–100152, https://doi.org/10.1016/j.cartre.2021.100116.
[40] Y. Lin, F. Lu, Y. Tu, Z. Ren, Glucose biosensors based on Carbon nanotube nanoelectrode ensembles, Nano Lett. 4 (2004) 191–195, https://doi.org/10.1021/nl0347233.
[41] S. Guo, X. Qu, S. Dong, Nanoelectrode ensembles based on semi-interpenetrating network of carbon nanotubes, Electrochim. Acta 52 (2007) 6186–6191, https://doi.org/10.1016/j.electacta.2007.04.018.
[42] B.V. Chikkaveeraiah, A. Bhirde, R. Malhotra, V. Patel, J.S. Gutkind, J.F. Rusling, Single-wall carbon nanotube forest arrays for immunoelectrochemical measurement of four protein biomarkers for prostate cancer, Anal. Chem. 81 (2009) 9129–9134, https://doi.org/10.1021/ac9018022.
[43] J. Huang, Y. Liu, T. You, Carbon nanofiber based electrochemical biosensors: a review, Anal. Methods 21 (2010) 202–209, https://doi.org/10.1039/B9AY00312F.
[44] Y. Song, H. Fan, M.J. Anderson, J.G. Wright, D.H. Hua, J. Koehne, M. Meyyappan, J. Li, Electrochemical activity assay for protease analysis using carbon nanofiber nanoelectrode arrays, Anal. Chem. 91 (2019) 3971–3979, https://doi.org/10.1021/acs.analchem.8b05189.
[45] C.M. Lentz, B.A. Samuel, H.C. Foley, M.A. Haque, Synthesis and characterization of glassy carbon nanowires, J. Nanomat. 2011 (2010) 129298–129306, https://doi.org/10.1155/2011/129298.
[46] C. Wang, Q. Liu, X. Shao, G. Yang, H. Xue, X. Hu, One step fabrication of nanoelectrode ensembles formed via amphiphilic block copolymer self-assembly and selective voltammetric detection of uric acid in the presence of high ascorbic acid content, Talanta 71 (2008) 178–185, https://doi.org/10.1016/j.talanta.2006.03.055.
[47] H.B. Habtamu, P. Ugo, Miniaturized enzymatic biosensor via biofunctionalization of the insulator of nanoelectrode ensembles, Electroanalysis 27 (2015) 2187–2193, https://doi.org/10.1002/elan.201500115.
[48] B. Strehlitz, B. Grundig, W. Schumacher, P.M.H. Kroneck, K.D. Vorlop, H. Kotte, A Nitrite sensor based on a highly sensitive nitrite reductase mediator-coupled amperometric detection, Anal. Chem. 68 (1996) 807–816, https://doi.org/10.1021/ac950692n.
[49] A. Lombardo, T.I. Bieber, Ferrocenyl methylation of aniline: non-kinetic determination of a reaction mechanism, J. Chem. Educ. 60 (1983) 1080–1081, https://doi.org/10.1021/ed060p1080.
[50] A.J. Bard, L.R. Faulkner, Electrochemical methods: fundamentals and applications, second ed., Wiley, New York, 2001.
[51] M. De Leo, A. Kuhn, P. Ugo, 3D-Ensembles of gold nanowires: preparation, characterization and electroanalytical peculiarities, Electroanalysis 19 (2007) 227–236, https://doi.org/10.1002/elan.200603724.
[52] D.M. Morales, M. Risch, Seven steps to reliable cyclic voltammetry measurements for the determination of double layer capacitance, J. Phys. Energy 3 (3) (2021), 034013, https://doi.org/10.1088/2515-7655/abee33.
[53] D. Voiry, M. Chhowalla, Y. Gogotsi, N.A. Kotov, Y. Li, R.M. Penner, R.E. Schaak, P.S. Weiss, Best practices for reporting electrocatalytic performance of nanomaterials, ACS Nano 12 (2018) 9635–9638, https://doi.org/10.1021/acsnano.8b07700.
[54] S. Ranganathan, T.-C. Kuo, R.L. McCreery, Facile preparation of active glassy carbon electrodes with activated carbon and organic solvents, Anal. Chem. 71 (16) (1999) 3574–3580, https://doi.org/10.1021/ac981386n.
[55] J. Xu, Q. Chen, G.M. Swain, Anthraquinonedisulfonate electrochemistry: a comparison of glassy carbon, hydrogenated glassy carbon, highly oriented pyrolytic graphite, and diamond electrodes, Anal. Chem. 70 (1998) 3146–3154, https://doi.org/10.1021/ac9800661.
[56] M.A. Beluomini, N. Karimian, N.R. Stradiotto, P. Ugo, Tailor-Made 3D-Nanoelectrode ensembles modified with molecularly imprinted poly(o-phenylenediamine) for the sensitive detection of L-arabitol, Sens. Actuators B Chem. 284 (2019) 250–257, https://doi.org/10.1016/j.snb.2018.12.091.
[57] O. Sliusarenko, A. Oleinick, I. Svir, C. Amatore, Validating a central approximation in theories of regular electrochemical arrays of various common geometries, Electroanalysis 27 (2015) 980–991, https://doi.org/10.1001/elan.201400593.
[58] N. Godino, X. Borrise, F.X. Munoz, F. Javier del Campo, R.G. Compton, Mass Transport to Nanoelectrode Arrays and Limitations of the Diffusion Domain Approach: Theory and Experiment, J. Phys. Chem. C 113 (2009) 11119–11125, https://doi.org/10.1021/jp9031354.